

Article

Robustness of the Skyrmion Phase in a Frustrated Heisenberg Antiferromagnetic Layer Against Lattice Imperfections and Nanometric Domain Sizes

Mariia Mohyl'na and Milan Žukovič * 

Department of Theoretical Physics and Astrophysics, Institute of Physics, Faculty of Science, Pavol Jozef Šafárik University in Košice, 041 54 Košice, Slovakia

* Correspondence: milan.zukovic@upjs.sk

Abstract: By employing GPU-implemented hybrid Monte Carlo simulations, we study the robustness of the skyrmion lattice phase (SkX) in a frustrated Heisenberg antiferromagnetic (AFM) layer on a triangular lattice with a Dzyaloshinskii–Moriya interaction in the external magnetic field against the presence of lattice imperfections (nonmagnetic impurities) and lattice finiteness. Both features are typical of experimentally accessible magnetic materials and require theoretical investigation. In the pure model of infinite size, SkX is known to be stabilized in a quite wide temperature-field window. We first study the effects of such imperfections on the SkX stability and compare them with those in the nonfrustrated ferromagnetic counterpart. The partial results of this part appeared in the conference proceedings [M. Mohyl'na and M. Žukovič, Proceedings of the 36th International ECMS International Conference on Modelling and Simulation, ECMS, 2022]. We further look into whether SkX can also persist in finite clusters, i.e., zero-dimensional systems of nanometric sizes. In general, both the presence of magnetic vacancies as well as the finiteness of the system tend to destabilize any ordering. We show that in the present model, SkX can survive, albeit in a somewhat distorted form, in the impure infinite system up to a fairly large concentration of impurities, and, in the pure finite systems, down to sizes comprising merely tens of particles. Distortion of the SkX phase due to the formation of bimerons, reported in the ferromagnetic model, was not observed in the present frustrated AFM case.

Keywords: Heisenberg antiferromagnet; geometrical frustration; skyrmion lattice; nonmagnetic impurities; finite-size cluster; hybrid Monte Carlo



Citation: Mohyl'na, M.; Žukovič, M. Robustness of the Skyrmion Phase in a Frustrated Heisenberg Antiferromagnetic Layer against Lattice Imperfections and Nanometric Domain Sizes. *Magnetochemistry* **2023**, *9*, 101. <https://doi.org/10.3390/magnetochemistry9040101>

Academic Editor: Shengcan Ma

Received: 15 March 2023

Revised: 31 March 2023

Accepted: 3 April 2023

Published: 6 April 2023



Copyright: © 2023 by the authors. Licensee MDPI, Basel, Switzerland. This article is an open access article distributed under the terms and conditions of the Creative Commons Attribution (CC BY) license (<https://creativecommons.org/licenses/by/4.0/>).

1. Introduction

Magnetic skyrmions, topologically nontrivial twisted magnetic spin configurations, have recently attracted a lot of attention due to their wide variety of properties, which make them promising candidates for the new generation of memory storage devices [1], logic gates [2], microwave detectors [3] and others [4–6]. Similar to the topological objects that have been well known for decades, i.e., domain walls and magnetic vortexes, skyrmions carry a certain property, called topological charge or topological number, which sets them apart from topologically trivial spin textures, such as ferromagnetic (FM) or antiferromagnetic (AFM) order, and distinguishes one topological object from another. The idea of the existence of topologically nontrivial structures in magnetic materials was actively theoretically developed at the end of the previous century [7–9], but it was not until 2009 that the first direct experimental proof of the presence of the hexagonal skyrmion crystal phase in a bulk ferromagnet was obtained by Mühlbauer et al. [10]. After that, the search for new skyrmion-hosting materials began in order to identify the most promising materials for technological implementation. They were found in Hall ferromagnets, ferromagnetic monolayers, multilayers and ferrimagnets.

The reason for the stabilization of the skyrmion lattice (SkX) state is usually the presence of a Dzyaloshinskii–Moriya interaction (DMI) [11,12], which breaks the inversion symmetry. Nevertheless, there are some other mechanisms that can lead to the formation of skyrmions, among which are frustrated interactions, which are of particular interest. It was recently demonstrated by Okubo et al. [13] that such interactions are capable of stabilizing both skyrmion and antiskyrmion crystals on any lattices of the trigonal symmetry with next-nearest interactions. Although skyrmions were first encountered in FM materials, recently the focus has shifted to the AFM materials [14–23], which were proven to be capable of hosting the SkX phase. In particular, it was shown by Rosales et al. [14] and Osorio et al. [17] that SkX can be stabilized in the classical Heisenberg AFM on a triangular lattice with moderate DMI in quite a wide temperature-field window due to the combined effects of the frustration and DMI. Further studies demonstrated the possibility of the SkX phase stabilization even at very small values of DMI [21,22]. In our very recent study, we showed the possibility of the emergence of an antiferromagnetic skyrmion/antiskyrmion lattice in this model even in the absence of DMI, providing that the exchange interactions are taken up to the third nearest neighbours [24].

The stability of skyrmions is guaranteed by topological charge as it is an invariant; however, in real materials, it is not absolute and thermal fluctuations can bring the system over the finite energy barrier, separating one spin configuration from another. Several works have studied the lifetime of skyrmions in thin films, multilayers and racetracks and the ways to improve their thermal stability, both theoretically [25–30] as well as experimentally [31–35]. Overall, a significant role in their stabilization has been ascribed to DMI. Another destabilization factor is the presence of nonmagnetic impurities (spin vacancies), which is a common feature in magnetic solids. In the case of frustrated spin systems with a ground-state degeneracy, the problem of collective impurity behaviour can become rather nontrivial due to a possible “order by quenched disorder” effect with a profound impact on the phase diagram. In particular, for the classical Heisenberg AFM on a triangular lattice in an external magnetic field but without DMI, it has been shown that competition between thermal fluctuations and nonmagnetic impurities leads to a complicated temperature-field phase diagram, with the emergence of a conical state at low temperatures [36]. A considerable effect of nonmagnetic impurities has also been observed in the nonfrustrated FM Heisenberg model on a square lattice in the field with DMI [37], which displays the SkX phase. In particular, it was found that even very tiny concentrations of vacancies induce the formation of bimerons in both helical (HL) and SkX states. In the considered system, they show up as elongated configurations similar to skyrmions with their disk-shaped central cores shared by two half disks separated by a rectangular stripe domain. The presence of bimerons is found to cause deformation of both the HL and SkX states. While in the former case, it occurs due to their appearance between the vacancies, thus breaking stripe domain structures, in the latter case, bimerons cause the skyrmion positions in the skyrmion lattice to change in a nontrivial way and decrease their overall number. The nonmagnetic impurities thus distort both the skyrmion configuration and the skyrmion lattice.

Most theoretical studies consider systems of infinite lattice sizes; however, the sizes and boundaries of the real finite-sized sample can also play a crucial role in the destruction of skyrmions. Several studies have investigated skyrmions stored inside a confined geometry, e.g., nanowires and nanodisks [4,5,38,39]. For example, by studying geometrical and physical conditions for skyrmion stability in a nanowire it was found that some minimum planar dimensions have to be satisfied to stabilize a skyrmion. In particular, skyrmions cannot be formed if both the length and width of a nanowire do not exceed certain values [39]. Similarly, in nanodisks of both circular and square shapes, the diameter or edge length have to exceed certain values in order to observe a complete skyrmion phase [40].

Therefore, it is very important to emulate the real materials used in experiments as closely as possible. Although a few studies on the Heisenberg AFM with DMI have already attempted to introduce some more realistic features, such as the presence of a single-ion anisotropy [41,42] or quantum effects [20], the effects of nonmagnetic impurities,

very common in real materials, and sample size effects remain to be investigated. In this work, we study the influence of nonmagnetic impurities and sample finiteness on the stability of the SkX phase in the frustrated classical Heisenberg AFM on a triangular lattice in the presence of DMI by means of hybrid Monte Carlo simulations. Since the problem is, in general, computationally very demanding and allows for parallelization, the simulations were implemented on a highly parallelized architecture of GPU using CUDA programming language.

2. Model and Methods

We investigated the classical Heisenberg AFM on a triangular lattice with the following Hamiltonian:

$$\mathcal{H} = -J \sum_{\langle i,j \rangle} \vec{S}_i \cdot \vec{S}_j + \sum_{\langle i,j \rangle} \vec{D}_{ij} \cdot [\vec{S}_i \times \vec{S}_j] - h \sum_i S_i^z, \quad (1)$$

where \vec{S}_i is a classical unit-length Heisenberg spin at the i th site, $J < 0$ is the AFM exchange coupling constant, h is the external magnetic field applied perpendicular to the lattice plane (along the z direction) and $\langle i, j \rangle$ denotes the sum over nearest-neighbour spins. \vec{D}_{ij} is the DMI vector whose orientation is defined by the crystal symmetries. In this study, we chose to point along the radius vector $\vec{r}_{ij} = \vec{r}_i - \vec{r}_j$ between two neighbouring sites, i.e., $\vec{D}_{ij} = D \frac{\vec{r}_{ij}}{|\vec{r}_{ij}|}$ (Figure 1), which results in the formation of Bloch-type skyrmions. The magnitude of the parameter D defines the strength of the DMI. The presence of nonmagnetic impurities is simulated by randomly replacing a certain percentage p of spins on the lattice with vacancies. In the following, we set $J = -1$ to fix the energy scale and absorb the Boltzmann constant in temperature by setting its value to $k_B = 1$.

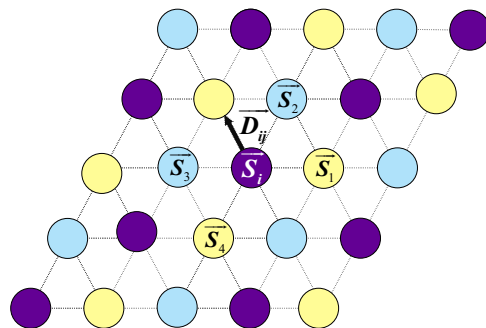


Figure 1. Three-sublattice decomposition of the triangular lattice shown by different colours. \vec{S}_i is the central spin, $\vec{S}_1, \dots, \vec{S}_4$ are the spins involved in the calculation of the local chirality and \vec{D}_{ij} represents the Dzyaloshinskii–Moriya vector.

Monte Carlo (MC) simulations are among the most powerful tools for studying the behaviour of magnetic materials at finite temperatures and, in particular, identifying the most promising candidates for the skyrmion-hosting environment. We applied this to the present model and calculated several relevant quantities. In particular, in order to identify the presence of the SkX phase, we used the skyrmion chirality, a discretization of a continuum topological charge [43], which reflects the number and the nature of topological objects present in the system. The topological charge of a single skyrmion is ± 1 for the core magnetization $\pm |\vec{S}|$ [44]. The skyrmion chirality κ is defined as follows:

$$\kappa = \frac{\langle K \rangle}{N} = \frac{1}{8\pi N} \left\langle \left| \sum_i (\kappa_i^{12} + \kappa_i^{34}) \right| \right\rangle, \quad (2)$$

where $\kappa_i^{ab} = \vec{S}_i \cdot [\vec{S}_a \times \vec{S}_b]$ is the chirality of a triangular plaquette of three neighbouring spins (area of the triangle spanned by those spins) and $\langle \dots \rangle$ denotes the thermal average. The chirality is calculated for the whole lattice and the summation runs through all the

spins with $\{\vec{S}_a, \vec{S}_b\}$ corresponding to $\{\vec{S}_1, \vec{S}_2\}$ and $\{\vec{S}_3, \vec{S}_4\}$ in Figure 1. Spins are taken in a counter-clockwise fashion to keep the sign in accordance with the rules in [43].

For the construction of the phase diagram, it is useful to calculate also some other basic thermodynamic quantities, such as the magnetization m and the specific heat c , as follows:

$$m = \frac{\langle M \rangle}{N} = \frac{1}{N} \left\langle \sum_i S_i^z \right\rangle, \quad (3)$$

$$c = \frac{\langle \mathcal{H}^2 \rangle - \langle \mathcal{H} \rangle^2}{NT^2}. \quad (4)$$

To identify the presence of the skyrmion phase and construct the phase diagrams, we implemented the hybrid Monte Carlo (HMC), which combines the standard Metropolis algorithm with the over-relaxation (OR) method [45]. The OR method is a deterministic energy-preserving perturbation method, which leads to the faster relaxation of the system due to faster decorrelation. To perform configurational averaging, we ran independent simulations on typically 50 replicas with different configurations of randomly distributed nonmagnetic impurities for each value of the impurity concentration p . In simulations, we used 2×10^6 MC sweeps, half of which were used for the equilibration. For diluted systems, the lattice size in all the simulations was $L = 48$ and periodic boundary conditions (PBC) were implemented. For finite-size clusters, the lattice size was varied within $9 \leq L \leq 120$ and open boundary conditions (OBC) were imposed. Parallel tempering Monte Carlo (PTMC) [46], which has been proven to be a much more efficient tool for the investigation of systems with complex energy landscapes and, in particular, skyrmion-hosting triangular Heisenberg antiferromagnets [22], was utilized for calculations at small DMI values. Due to high computational demands, the simulations were carried out on general-purpose Graphical Processing Units (GPGPU) using CUDA, which allowed for the massive parallelization of the calculations.

3. Results and Discussion

3.1. Effect of Impurities

The frustrated Heisenberg AFM with DMI has been previously intensively studied in a wide parameter space [14,21,22,47]. The phase diagram of a pure isotropic model with a moderate DMI ($0.2 < D < 1$) consists of three distinct phases: the helical (HL) phase with chiral stripes rotating in the x - y plane; the skyrmion lattice (SkX) phase, which consists of three interpenetrating skyrmion lattices on each of the sublattices; and the V-like (VL) phase [22]. The typical snapshots of the HL and the SkX phases on one of the sublattices in the case of no impurities are depicted in Figure 2a,b, respectively. The colours represent the values of the z -component: the red spins are those pointing along the external magnetic field and the blue ones are pointing opposite to it. The arrows show the projections of the spins to the x - y plane. The representative phase diagram for the model without impurities with $D = 0.5$ is shown in Figure 3 in black circles. The SkX phase occupies a relatively big part of the T - h plane and emerges at the fields around $h \approx 2.4$ for the lowest temperature, which is reflected in a sharp increase in the chirality, signalling the first-order phase transition [14] (see also Figure 4a below). The increase in temperature results in some distortion of the skyrmions' profile and, consequently, it leads to a smoothing of the chirality and the change of the transition type to a second-order one [22].

We note that the presence of the VL phase was identified by Osorio et al. [17] by using the effective low-energy theory (they called it the sublattice uniform SU phase, obeying the sublattice spins constraint $\vec{S}_1 + \vec{S}_2 + \vec{S}_3 = \vec{h}/3$); however, it is rather difficult to reliably determine its boundaries by MC simulations. As shown in Figure 3, it appears within the field window above the SkX phase, i.e., with zero chirality and below the fully polarized phase, i.e., with the magnetization not yet fully saturated. The problematic part is the determination of the lower-field boundary due to the fact that, as can be seen from Figure 4a, the chirality vanishes in a step-wise fashion (there are also multiple anomalies in other quantities), which can be attributed to the finiteness of the lattice. A crossover

to a continuous behaviour, with the inflection point in the chirality and singularity in the chiral susceptibility at the transition point, would only be observed if the lattice size was taken to infinity. That would, however, require a time-consuming finite-size scaling analysis considering very large lattice sizes. For the purpose of the present paper, we approximately identify the VL phase as the region between the beginning of the last step in the vanishing chirality and the fully polarized state with $m = m_{sat}$. This, admittedly arbitrary, criterion is supported by the visual inspection of the spin snapshots. Similar to the other phase transitions occurring at very low temperatures, the transition to the VL phase is also difficult to localize from the specific heat peak, as the latter is usually too narrow to be captured in MC simulations.

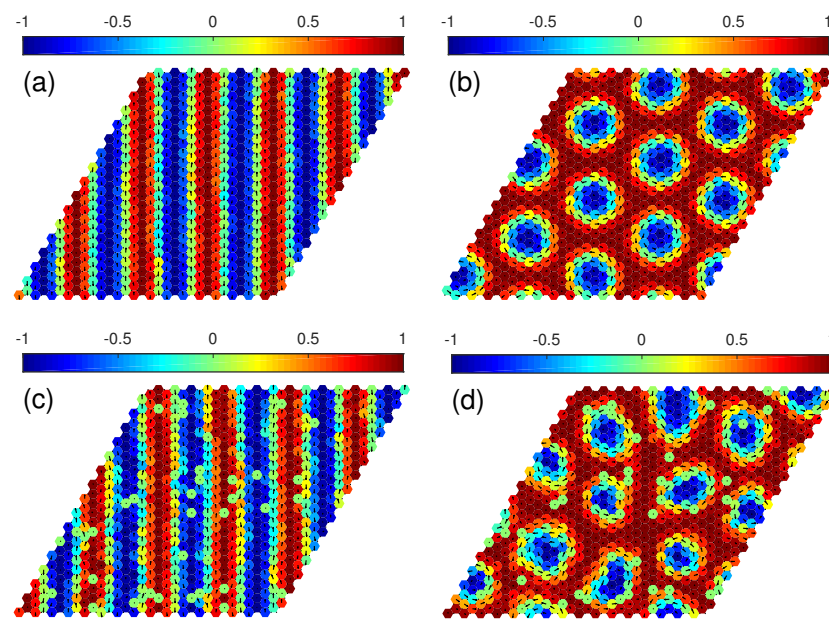


Figure 2. (a,c) HL states at $h = 1.6$ and (b,d) SkX states at $h = 2.4$ for (a,b) pure system and (c,d) with $p = 5\%$ of vacancies. The remaining parameters are $T = 0.01$, $D = 0.5$ and $L = 48$. The green circles in (c,d) represent the vacancy locations. The snapshots are taken for one of the replicas.

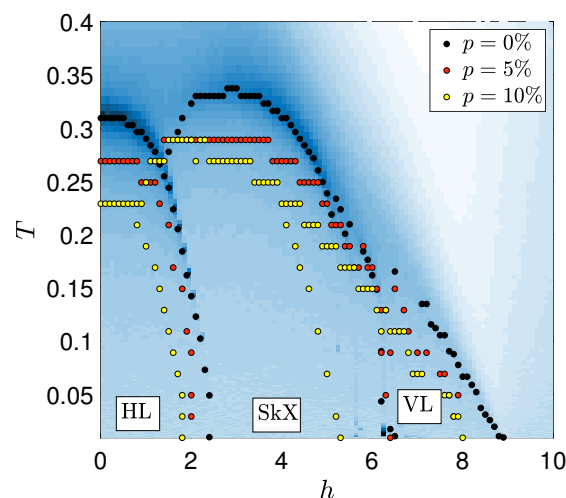


Figure 3. Phase diagrams of the Heisenberg AFM model in $T - h$ plane with $D = 0.5$ and different p . The black, red and yellow circles represent the cases with $p = 0\%$, 5% and 10% , respectively. The phase diagrams were constructed using the information from the chirality, magnetization, the peaks in the specific heat as well as the direct observation of the snapshots. The phase boundaries are overlaid on the specific heat plot for the case of $p = 0\%$.

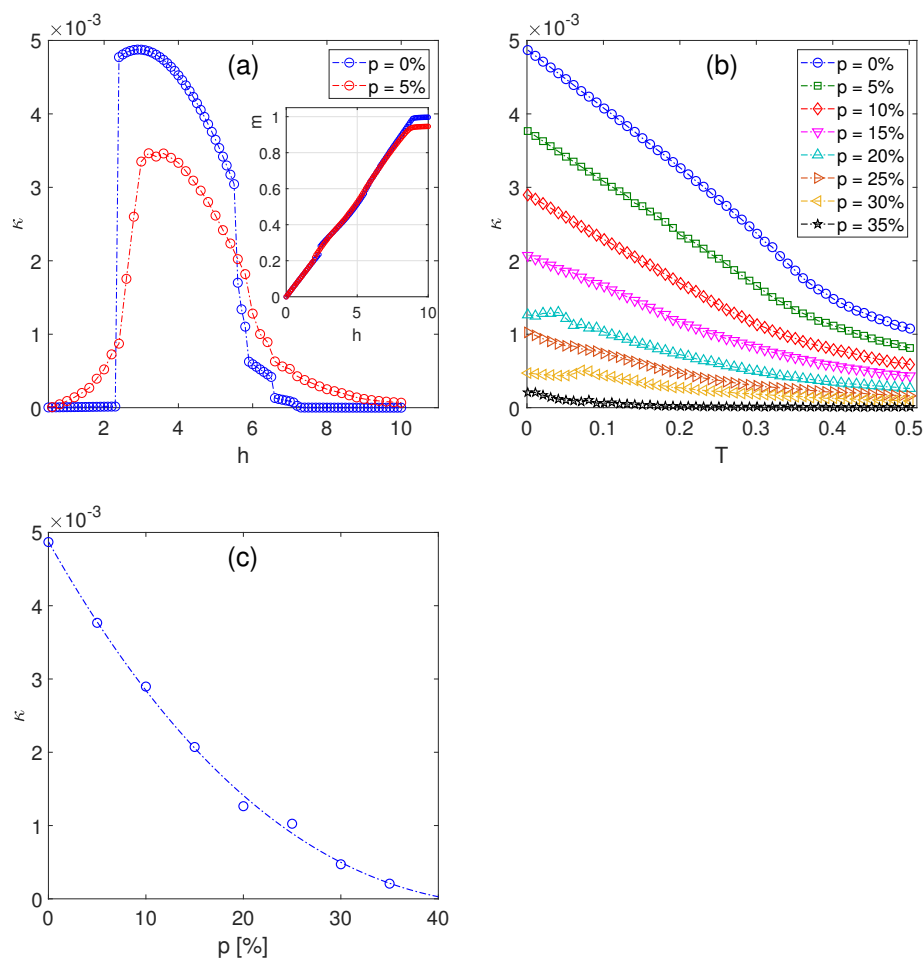


Figure 4. (a) Field dependencies of the chirality and magnetization (in inset) for two values of p at $T = 0.01$ and (b) temperature dependencies of the chirality at $h = 3.4$, for selected values of the concentration of nonmagnetic vacancies p . (c) The chirality at $T = 0.001$ as a function of p . The dash-dotted curve is obtained by fitting.

To simulate the presence of nonmagnetic impurities in our system, we randomly replaced $p\%$ of the sites with vacancies and studied their effect on the HL and SkX states. In Figure 2, we present the respective states in the pure system (a,b) and with $p = 5\%$ of nonmagnetic impurities (c,d) on one of the three interpenetrating sublattices in the HL phase (a,c) and the SkX phase (b,d). The snapshots for one of the running replicas are shown. We can observe that, compared to the pure systems, the presence of the vacancies naturally results in some distortion of the respective phases. Nevertheless, there are no signs of the formation of bimerons, as was the case in the FM model [37]. We believe that the present AFM system is more resilient against the creation of bimerons than the FM one due to the fact that both HL and SkX textures are formed on each of the three interpenetrating sublattices. Therefore, for example, the stripe domain structures in the HL state are more robust and it is more difficult for nonmagnetic impurities to break them into pieces (bimerons) than in the FM system. Naturally, with the increasing concentration of impurities, the HL phase will eventually become distorted as well. Nevertheless, in comparison with the SkX phase, it appears slightly more robust against the impurities. We speculate that it might be due to the fact that, in the HL phase, the spins in similar states form compact bands that stretch across the entire lattice. On the other hand, the skyrmions are more vulnerable since they are isolated from each other and, as described below, their edges tend to conform to locations of vacancies.

In the SkX phase, one can notice that, besides the skyrmion distortion, the presence of vacancies also reduces their number. It is interesting to study their mutual interaction. It is

known that isolated skyrmions in isotropic 2D Heisenberg magnets are attracted to the spin vacancies [48,49], which allows there to be an impurity at a skyrmion centre. On the other hand, skyrmions in a skyrmion crystal do not generally appear centred at vacancies. In such a case, it is energetically more favourable if the skyrmion lattice is formed in such a way that the spin vacancies become, in general, localized between skyrmions [37]. This phenomenon can be also observed in the present case (see Figure 2d), when the skyrmions tend to rearrange in such a way that the vacancies stay at their outskirts. We also checked the states involving larger-size skyrmions (generated by smaller DMI) and observed basically the same behaviour. Namely, the skyrmions formed in such a way that they avoid vacancies in their interiors, albeit some isolated vacancies may also sporadically appear in their cores. As a result, they may become elongated or otherwise disfigured, which prevents their optimal compact regular hexagonal arrangement on the lattice and consequently reduces the number of skyrmions that can fit on the lattice.

In Figure 4, we plot field and temperature dependencies of the chirality for selected values of the concentration of nonmagnetic vacancies p . The presence of impurities leads to a distortion of the skyrmion profiles and, consequently, a reduction in the magnitude of the chirality. At the same time, it smears out its abrupt change, particularly at the HL-SkX phase transition, with smaller but finite values within the higher-field part of the HL phase (see Figure 4a). The effect of the chirality reduction with the increasing concentration of the nonmagnetic impurities is also demonstrated in Figure 4b, in which the chirality is plotted versus temperature for a wide range of concentrations p . A similar effect of distortion of the skyrmion profiles and a reduction in the chirality is also produced by thermal fluctuations.

The phase diagrams for $p = 5\%$ (red circles) and $p = 10\%$ (yellow circles) are presented in Figure 3. Their overall topology remains unchanged as compared to the case of the pure model and consists of the HL phase in the low-field region, the VL phase in the high-field region and the SkX phase sandwiched between them. However, a tendency of the SkX phase to shrink and smear with the increasing number of impurities can be noticed. Nevertheless, the area of the SkX phase still occupies a big part of the phase diagram even for $p = 10\%$.

As suggested by Figures 3 and 4b, with the gradual increase in dilution, the number of skyrmions decreases, and also the corresponding transition temperature from the SkX to paramagnetic (P) phase drops. From Figure 4c, it is evident that skyrmions (non-zero chirality) can survive to at least $p = 35\%$, which is the threshold value estimated for the FM model on the square lattice [37]. In fact, we found out that the chirality remains finite even well above $p = 35\%$; however, the skyrmions become considerably disfigured and visually difficult to identify. Thus, a more precise value of the threshold concentration for the present model is rather difficult to estimate. From our results, it follows that, for the considered model parameters $D = 0.5$ and $h = 3.4$, the skyrmion phase cannot survive if the concentration of nonmagnetic impurities exceeds $p_c \gtrsim 35\%$. We should remark that such high concentrations of impurities may seriously affect also other model parameters and calling the phase with just a few highly distorted skyrmions on the whole lattice the skyrmion lattice phase might be questionable. On the other hand, we need to set some criteria for the existence of the SkX phase, based on the order parameter. Then, if the chirality is chosen to be one, then the concentration at which it vanishes would indeed be close to $p_c \gtrsim 35\%$.

There are some suggestions that the value of p_c may change with D . It is known that for the pure case, the transition temperature from the SkX to P phase increases with the increase in D [22]. If this relation also holds for the diluted model, then the SkX phase may survive to larger values of p if the DMI is increased. In Figure 5, we plot the SkX-P transition temperatures T_c^{SkX} as functions of p for $D = 0.5$ and 1. The values are just rough estimates, obtained for a finite-size system based on the specific heat maxima positions, and thus the phase diagrams should be read rather qualitatively. Moreover, with increasing p , the peaks become smeared, and for $p \gtrsim 35\%$ they are difficult to localize. Nevertheless,

it is apparent that $T_c^{SkX}(D = 1) > T_c^{SkX}(D = 0.5)$ within the whole range of $0 \leq p \leq 0.35$, and thus it is quite possible (but not inevitable) that $p_c(D = 1) > p_c(D = 0.5)$.

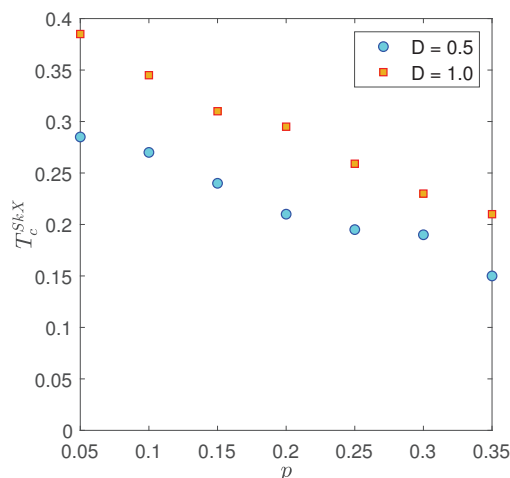


Figure 5. Phase diagrams of the Heisenberg AFM model in $T - p$ plane with $h = 3.4$ and different values of D . T_c^{SkX} represents transition temperatures between SkX and P phases.

3.2. Lattice Finiteness

In the following, we study the properties of the system on finite spin clusters, which are realized in MC simulations by imposing OBC. Particularly we focus on the question of whether the SkX phase can also be stabilized in such systems, and if so whether there is a minimal size for the domains that would still support the formation of skyrmions. We consider nanoclusters and nanoparticles that involve a number of spins ranging from tens to tens of thousands.

In Figure 6, we present the temperature dependencies of the specific heat for $D = 0.5$, $h = 3.4$ and various lattice sizes $L = 24, \dots, 108$ with OBC, including the case of $L = 48$ with PBC. One can see that the maxima signifying the phase transitions to the SkX phase are still present, albeit OBC make them lower and rounder when compared to those with the same size but PBC. Naturally, the increasing L tends to diminish the differences, since in the limit of $L \rightarrow \infty$, the boundary conditions become irrelevant. The finite values of the chirality as well as spin snapshots in the low-temperature region clearly showing the presence of skyrmions (the chirality due to lattice finiteness remains finite even at higher temperatures, however there are no skyrmions) (see Figure 6b) corroborate our expectations that the area below the peaks in the specific heat curves corresponds to the SkX phase. It is interesting to see a relatively large scatter of the saturation values of the chirality achieved at the lowest temperature for different L . The differences, apparently, result from the (non)commensurability of the total number of skyrmions and the lattice size. Namely, the chosen parameters $D = 0.5$ and $h = 3.4$ generate skyrmions of some characteristic size [22], which try to fill the entire lattice in the hexagonal arrangement. Considering these constraints, smaller lattices are rather rigid and may only allow the formation of a very small number of skyrmions (see the snapshot for $L = 24$), while larger sizes are more flexible and can accommodate a much greater number of skyrmions (see the snapshot for $L = 48$). However, with the increase in L , the saturation values seem to converge to some common value corresponding to the case of $L \rightarrow \infty$, partially emulated by imposing PBC.

So, apparently, the SkX phase can also be stabilized in finite spin clusters. However, the clusters should be large enough to allow the formation of skyrmions. From the discussion above, one would expect that the minimal cluster size displaying the SkX phase should depend on DMI. In particular, for larger D , the very small skyrmions should survive in rather small clusters, while giant skyrmions produced at very small D would require much large cluster sizes. In Figure 7, we demonstrate that for $D = 1$, skyrmions can be formed even in the cluster with $L = 9$. At low temperatures, the chirality still acquires finite values

and the specific heat displays an anomaly, marking the high-temperature onset of the SkX phase formation. The snapshot illustrates the presence of a single whole skyrmion with a minimal size involving seven spins. Namely, it is formed by one central spin pointing against the field direction, being surrounded by its six nearest neighbours that form a whirl in the x - y plane.

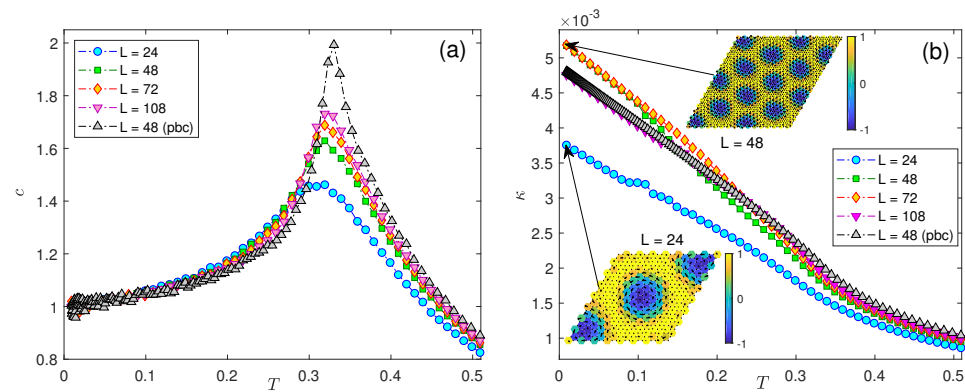


Figure 6. Temperature dependencies of (a) the specific heat and (b) the chirality for $D = 0.5$, $h = 3.4$ and several values of the lattice size L .

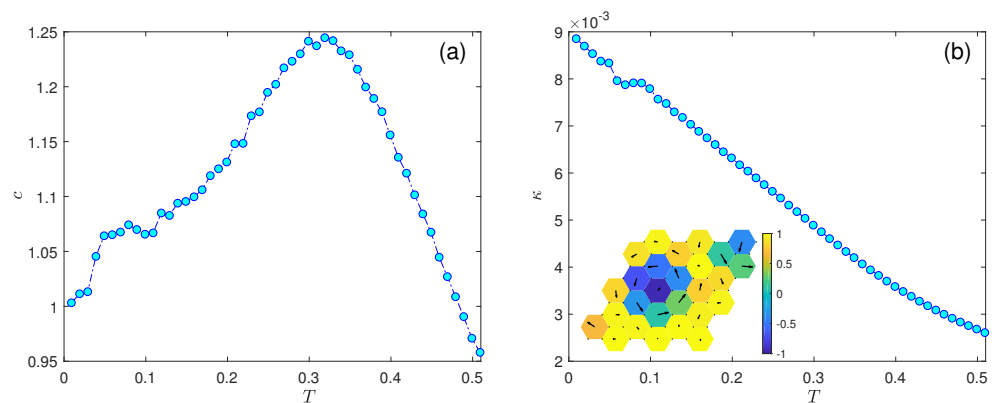


Figure 7. Temperature dependencies of (a) the specific heat and (b) the chirality for $D = 1$, $h = 3.4$ and $L = 9$.

In the systems with PBC, the presence of skyrmions was confirmed down to $D = 0.04$ for $L = 120$ and extrapolated to $D \approx 0.02$ for $L \rightarrow \infty$ [22]. Apparently, for finite clusters, much larger values of DMI are required to stabilize the SkX phase. Figure 8a demonstrates that for $D = 0.04$, the clusters of the size $L = 120$ do not undergo the transition from the up-up-down to the SkX phase, as we witnessed in the PBC systems, but remain in the up-up-down state. Upon increase in either L (Figure 8b) or D (Figure 8c), there is a crossover to a peculiar state with one spin-up sublattice and two sublattices, each including rather large spin-up and spin-down domains. The increase in the cluster size to $L = 120$ at the same $D = 0.07$ results in the extension of the domain-like structure to all three sublattices (Figure 8d). These domains resemble fractions of deformed skyrmions; however, the total chirality remains close to zero. Further increase in D and L (Figure 8e,f) leads to the appearance of whole skyrmion-like structures but they are still rather deformed and scattered on the respective sublattices. Only for $D = 0.15$ and $L = 90$ one can observe almost circular-shaped skyrmions showing more or less regular arrangements on the sublattices and the case of $D = 0.20$ and $L = 90$ looks already like a typical configuration in the SkX phase.

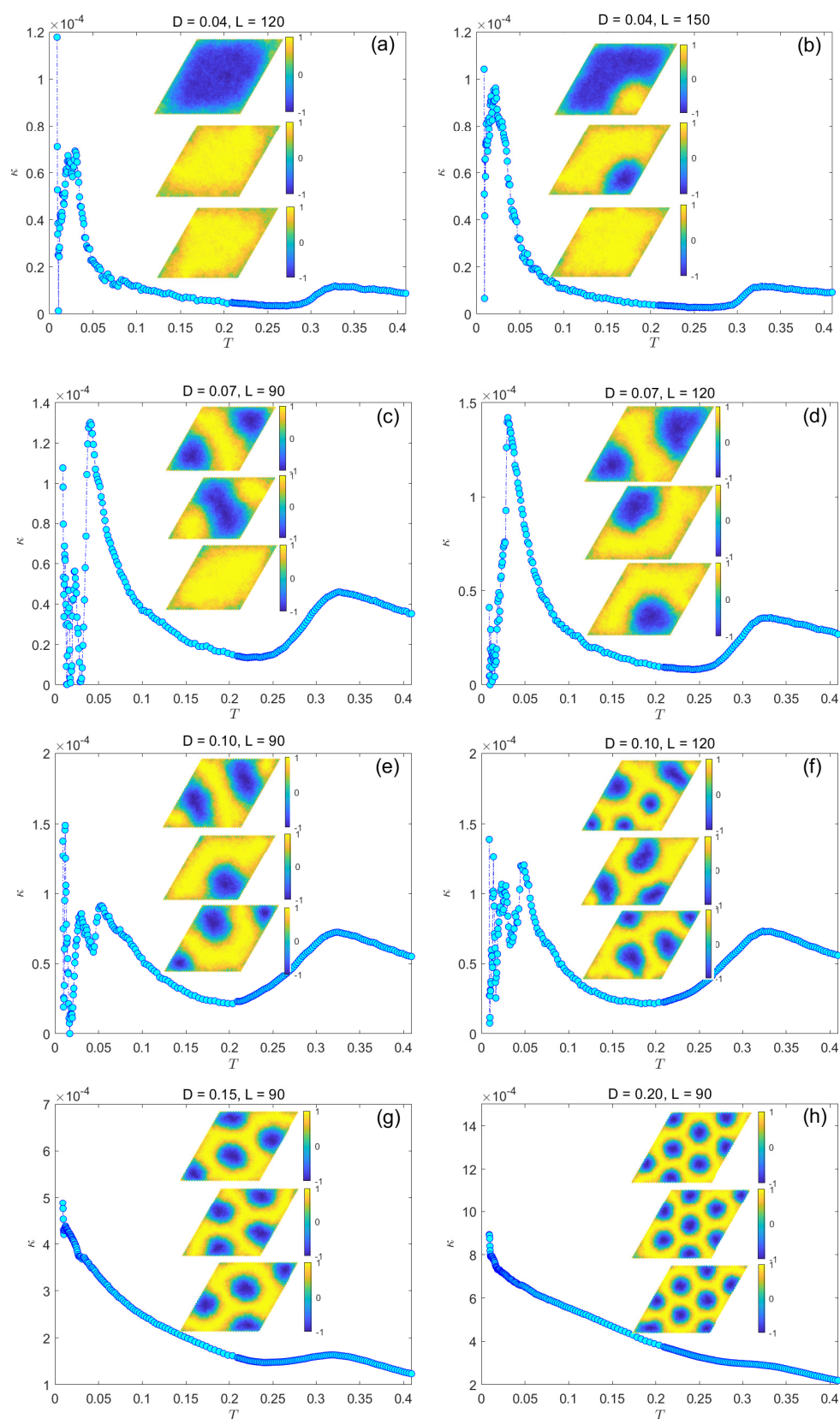


Figure 8. (a–h) Temperature dependencies of the chirality at $h = 3.2$ for various values of D and L . The snapshots show the evolution of spin configurations with the gradual increase in D and L on the three sublattices at the lowest temperature $T = 0.009$ (for clarity only the z -components of spins, in different colours, are shown).

It is interesting to observe a small but systematic increase in the chirality with the decreasing temperature in Figure 8a–f, without eventually reaching the SkX phase. We studied the evolution of the states by inspecting spin snapshots with the decreasing temperature and we found the following: In the region of the increasing chirality, we observed the persistence of the up-up-down phase, such as in the snapshots shown in Figure 8a. We conclude that the small increase in the chirality can be attributed to the arrangement of the spins at the perimeter. Namely, due to the free boundary conditions and small but non-zero DMI, instead of pointing up or down they start forming a giant whirl in the x - y plane (this can also be seen in Figure 8a). The spin-down sublattice could be considered as the core of a giant skyrmion, the characteristic size of which exceeds the size of the lattice. Such a state persists until the temperatures at which the chirality reaches its maximum are reached. At that point, such compact spin domains break into pieces (on either two or all three sublattices), and at still lower temperatures the typical states resemble those shown in Figure 8b–f for the lowest temperature.

4. Conclusions

We investigated the effects of the presence of nonmagnetic impurities and constraints imposed by lattice finiteness in the frustrated Heisenberg AFM model with the DMI hosting the SkX phase. The purpose of the first part was to confront the effects of impurities on the HL and SkX phases in the present frustrated AFM model with those observed in the nonfrustrated FM model [37], and also to take into account a more realistic situation in the possible experimental realizations of the present model [41]. We focused on the influence of impurities on the shape, size and position of individual skyrmions on the lattice as well as the overall stability of the SkX phase. Our findings suggest that both the HL and the SkX phases in the present frustrated AFM system are more robust against distortion, induced by those impurities, than in the nonfrustrated FM counterpart, where the formation of bimerons already occurs at low concentrations of $p \approx 1\%$. In our case, the skyrmion lattice is formed so that the vacancies become localized between the skyrmions. The effect caused by the presence of impurities is similar to the one caused by thermal fluctuations: the skyrmion's shape is distorted and the chirality is both reduced and smeared out, in particular at the HL-SkX phase boundary. This tendency becomes more pronounced with the increasing percentage of impurities. We estimate that the threshold below which no SkX phase can be stabilized is $p_c \approx 35\%$ for the selected value of $D = 0.5$, but it might increase for larger D .

We found that SkX can also exist in finite spin clusters as long as the DMI is sufficiently large to allow its stabilization. For large values of DMI ($D \gtrsim 1$), the characteristic size of the skyrmions is very small and thus SkX can be realized even in nanoclusters involving only tens of spins. On the other hand, relatively small values of DMI ($0.02 \lesssim D \lesssim 0.1$) that support the formation of SkX in the infinite system may not be sufficient to stabilize SkX, even in rather large but finite clusters. Thus, the minimal value of DMI at which the regular SkX phase in the finite cluster appears is about one order of magnitude larger than in the infinite system. Finally, we should note that the present investigations were performed at some fixed values of the external magnetic field at which the SkX phase was confirmed in the infinite system and focused on the low-temperature region. However, the field-temperature window of the SkX phase stabilization shrinks with the decreasing DMI, not only in the infinite system but also in the case of finite clusters. Therefore, at small DMI, even if the SkX phase exists, it might be difficult practically to localize it.

Finally, the studied model could be applicable to a 2D AFM system, for example based on TMDs proposed by Fang et al. [41]. In this case, the realistic effects, such as the corresponding magnitudes of DMI and anisotropy, should be properly accounted for. In fact, the effects of DMI and anisotropy in this model have previously been studied [22,42]. In the present paper, we chose to focus on some other attributes of realistic systems, i.e., the presence of impurities and the finite size. We did not target any specific realization and thus, for simplicity, we considered only the DMI (essential for the emergence of SkX)

within some range of magnitudes and disregarded the effects of anisotropy. The aim was to demonstrate the quite impressive stability of the AFM SkX phase against impurities (as compared to FMs) and to show that it can also be stabilized in finite clusters. Further, we believe that the application of this model, considering all relevant realistic conditions, to study some promising candidates for the AFM SkX phase realization would be interesting.

Author Contributions: M.M.: investigation, software, data curation, validation, visualization, writing—original draft. M.Ž.: conceptualization, methodology, validation, preparing the manuscript, supervision, writing—reviewing and editing, project administration, funding acquisition. All authors have read and agreed to the published version of the manuscript.

Funding: This research was funded by Vedecká Grantová Agentúra MŠVVaŠ SR a SAV (grant number 1/0695/23) and Agentúra na Podporu Výskumu a Vývoja (grant number APVV-SK-CZ-RD-21-0114).

Institutional Review Board Statement: Not applicable.

Informed Consent Statement: Not applicable.

Data Availability Statement: Not applicable.

Conflicts of Interest: The authors declare no conflict of interest.

References

1. Zhang, X.; Zhao, G.; Fangohr, H.; Liu, J.P.; Xia, W.; Xia, J.; Morvan, F. Skyrmion-skyrmion and skyrmion-edge repulsions in skyrmion-based racetrack memory. *Sci. Rep.* **2015**, *5*, 7643. [[CrossRef](#)] [[PubMed](#)]
2. Zhang, X.; Ezawa, M.; Zhou, Y. Magnetic skyrmion logic gates: Conversion, duplication and merging of skyrmions. *Sci. Rep.* **2015**, *5*, 9400. [[CrossRef](#)] [[PubMed](#)]
3. Finocchio, G.; Ricci, M.; Tomasello, R.; Giordano, A.; Lanuzza, M.; Puliafito, V.; Burrascano, P.; Azzaroni, B.; Carpentieri, M. Skyrmion based microwave detectors and harvesting. *Appl. Phys. Lett.* **2015**, *107*, 262401. [[CrossRef](#)]
4. Sampaio, J.; Cros, V.; Rohart, S.; Thiaville, A.; Fert, A. Nucleation, stability and current-induced motion of isolated magnetic skyrmions in nanostructures. *Nat. Nanotechnol.* **2013**, *8*, 839. [[CrossRef](#)]
5. Fert, A.; Cros, V.; Sampaio, J. Skyrmions on the track. *Nat. Nanotechnol.* **2013**, *8*, 152–156. [[CrossRef](#)]
6. Schulz, T.; Ritz, R.; Bauer, A.; Halder, M.; Wagner, M.; Franz, C.; Pfleiderer, C.; Everschor, K.; Garst, M.; Rosch, A. Emergent electrodynamics of skyrmions in a chiral magnet. *Nat. Phys.* **2012**, *8*, 301–304. [[CrossRef](#)]
7. Belavin, A.; Polyakov, A. Metastable states of two-dimensional isotropic ferromagnets. *JETP Lett.* **1975**, *22*, 245–248.
8. Bogdanov, A.; Yablonskii, D. Thermodynamically stable “vortices” in magnetically ordered crystals. The mixed state of magnets. *Zh. Eksp. Teor. Fiz.* **1989**, *95*, 182.
9. Roessler, U.K.; Bogdanov, A.; Pfleiderer, C. Spontaneous skyrmion ground states in magnetic metals. *Nature* **2006**, *442*, 797–801. [[CrossRef](#)]
10. Mühlbauer, S.; Binz, B.; Jonietz, F.; Pfleiderer, C.; Rosch, A.; Neubauer, A.; Georgii, R.; Böni, P. Skyrmion lattice in a chiral magnet. *Science* **2009**, *323*, 915–919. [[CrossRef](#)]
11. Dzyaloshinsky, I. A thermodynamic theory of “weak” ferromagnetism of antiferromagnetics. *J. Phys. Chem. Solids* **1958**, *4*, 241–255. [[CrossRef](#)]
12. Moriya, T. Anisotropic superexchange interaction and weak ferromagnetism. *Phys. Rev.* **1960**, *120*, 91. [[CrossRef](#)]
13. Okubo, T.; Chung, S.; Kawamura, H. Multiple- q states and the skyrmion lattice of the triangular-lattice Heisenberg antiferromagnet under magnetic fields. *Phys. Rev. Lett.* **2012**, *108*, 017206. [[CrossRef](#)]
14. Rosales, H.D.; Cabra, D.C.; Pujol, P. Three-sublattice skyrmion crystal in the antiferromagnetic triangular lattice. *Phys. Rev. B* **2015**, *92*, 214439. [[CrossRef](#)]
15. Leonov, A.; Mostovoy, M. Multiply periodic states and isolated skyrmions in an anisotropic frustrated magnet. *Nat. Commun.* **2015**, *6*, 8275. [[CrossRef](#)]
16. Barker, J.; Tretiakov, O.A. Static and dynamical properties of antiferromagnetic skyrmions in the presence of applied current and temperature. *Phys. Rev. Lett.* **2016**, *116*, 147203. [[CrossRef](#)]
17. Osorio, S.A.; Rosales, H.D.; Sturla, M.B.; Cabra, D.C. Composite spin crystal phase in antiferromagnetic chiral magnets. *Phys. Rev. B* **2017**, *96*, 024404. [[CrossRef](#)]
18. Bessarab, P.; Yudin, D.; Gulevich, D.; Wadley, P.; Titov, M.; Tretiakov, O.A. Stability and lifetime of antiferromagnetic skyrmions. *Phys. Rev. B* **2019**, *99*, 140411. [[CrossRef](#)]
19. Mutter, T.T.; Leonov, A.O.; Inoue, K. Skyrmion instabilities and distorted spiral states in a frustrated chiral magnet. *Phys. Rev. B* **2019**, *100*, 060407. [[CrossRef](#)]

20. Liu, Z.; dos Santos Dias, M.; Lounis, S. Theoretical investigation of antiferromagnetic skyrmions in a triangular monolayer. *J. Phys. Condens. Matter* **2020**, *32*, 425801. [[CrossRef](#)]
21. Mohylina, M.; Žukovič, M. Emergence of a Skyrmion Phase in a Frustrated Heisenberg Antiferromagnet with Dzyaloshinskii-Moriya Interaction. *Acta Phys. Pol. A* **2020**, *137*. [[CrossRef](#)]
22. Mohylina, M.; Buša Jr, J.; Žukovič, M. Formation and growth of skyrmion crystal phase in a frustrated Heisenberg antiferromagnet with Dzyaloshinskii-Moriya interaction. *J. Magn. Magn. Mater.* **2021**, *527*, 167755. [[CrossRef](#)]
23. Mohylina, M.; Tkachenko, V.; Žukovič, M. Road to zero-field antiferromagnetic skyrmions in a frustrated AFM/FM heterostructure. *Phys. Lett. A* **2022**, *449*, 128350. [[CrossRef](#)]
24. Mohylina, M.; Albarracín, F.G.; Žukovič, M.; Rosales, H. Spontaneous antiferromagnetic skyrmion/antiskyrmion lattice and spiral spin-liquid states in the frustrated triangular lattice. *Phys. Rev. B* **2022**, *106*, 224406. [[CrossRef](#)]
25. Rohart, S.; Miltat, J.; Thiaville, A. Path to collapse for an isolated Néel skyrmion. *Phys. Rev. B* **2016**, *93*, 214412. [[CrossRef](#)]
26. Rózsa, L.; Simon, E.; Palotás, K.; Udvardi, L.; Szunyogh, L. Complex magnetic phase diagram and skyrmion lifetime in an ultrathin film from atomistic simulations. *Phys. Rev. B* **2016**, *93*, 024417. [[CrossRef](#)]
27. Lobanov, I.S.; Jónsson, H.; Uzdin, V.M. Mechanism and activation energy of magnetic skyrmion annihilation obtained from minimum energy path calculations. *Phys. Rev. B* **2016**, *94*, 174418. [[CrossRef](#)]
28. Stosic, D.; Mulkers, J.; Van Waeyenberge, B.; Ludermit, T.B.; Milošević, M.V. Paths to collapse for isolated skyrmions in few-monolayer ferromagnetic films. *Phys. Rev. B* **2017**, *95*, 214418. [[CrossRef](#)]
29. Bessarab, P.F.; Müller, G.P.; Lobanov, I.S.; Rybakov, F.N.; Kiselev, N.S.; Jónsson, H.; Uzdin, V.M.; Blügel, S.; Bergqvist, L.; Delin, A. Lifetime of racetrack skyrmions. *Sci. Rep.* **2018**, *8*, 3433. [[CrossRef](#)]
30. Derras-Chouk, A.; Chudnovsky, E.M.; Garanin, D.A. Thermal collapse of a skyrmion. *J. Appl. Phys.* **2019**, *126*, 083901. [[CrossRef](#)]
31. Peng, L.; Zhang, Y.; Ke, L.; Kim, T.H.; Zheng, Q.; Yan, J.; Zhang, X.G.; Gao, Y.; Wang, S.; Cai, J.; et al. Relaxation dynamics of zero-field skyrmions over a wide temperature range. *Nano Lett.* **2018**, *18*, 7777–7783. [[CrossRef](#)]
32. Kindervater, J.; Stasinopoulos, I.; Bauer, A.; Haslbeck, F.X.; Rucker, F.; Chacon, A.; Mühlbauer, S.; Franz, C.; Garst, M.; Grundler, D.; et al. Weak crystallization of fluctuating skyrmion textures in MnSi. *Phys. Rev. X* **2019**, *9*, 041059. [[CrossRef](#)]
33. Birch, M.; Takagi, R.; Seki, S.; Wilson, M.; Kagawa, F.; Štefančič, A.; Balakrishnan, G.; Fan, R.; Steadman, P.; Ottley, C.; et al. Increased lifetime of metastable skyrmions by controlled doping. *Phys. Rev. B* **2019**, *100*, 014425. [[CrossRef](#)]
34. Crisanti, M.; Birch, M.; Wilson, M.; Moody, S.; Štefančič, A.; Huddart, B.; Cabeza, S.; Balakrishnan, G.; Hatton, P.; Cubitt, R. Position-dependent stability and lifetime of the skyrmion state in nickel-substituted Cu₂OSeO₃. *Phys. Rev. B* **2020**, *102*, 224407. [[CrossRef](#)]
35. Shimojima, T.; Nakamura, A.; Yu, X.; Karube, K.; Taguchi, Y.; Tokura, Y.; Ishizaka, K. Nano-to-micro spatiotemporal imaging of magnetic skyrmion's life cycle. *Sci. Adv.* **2021**, *7*, eabg1322. [[CrossRef](#)]
36. Maryasin, V.; Zhitomirsky, M. Triangular antiferromagnet with nonmagnetic impurities. *Phys. Rev. Lett.* **2013**, *111*, 247201. [[CrossRef](#)]
37. Silva, R.; Secchin, L.; Moura-Melo, W.; Pereira, A.; Stamps, R. Emergence of skyrmion lattices and bimerons in chiral magnetic thin films with nonmagnetic impurities. *Phys. Rev. B* **2014**, *89*, 054434. [[CrossRef](#)]
38. Iwasaki, J.; Mochizuki, M.; Nagaosa, N. Current-induced skyrmion dynamics in constricted geometries. *Nat. Nanotechnol.* **2013**, *8*, 742–747. [[CrossRef](#)] [[PubMed](#)]
39. Chui, C.; Ma, F.; Zhou, Y. Geometrical and physical conditions for skyrmion stability in a nanowire. *AIP Adv.* **2015**, *5*, 047141. [[CrossRef](#)]
40. Beg, M.; Chernyshenko, D.; Bisotti, M.A.; Wang, W.; Albert, M.; Stamps, R.L.; Fangohr, H. Finite size effects, stability, hysteretic behaviour, and reversal mechanism of skyrmionic textures in nanostructures. *arXiv* **2013**, arXiv:1312.7665.
41. Fang, W.; Raeliarijaona, A.; Chang, P.H.; Kovalev, A.A.; Belashchenko, K.D. Spirals and skyrmions in antiferromagnetic triangular lattices. *Phys. Rev. Mater.* **2021**, *5*, 054401. [[CrossRef](#)]
42. Mohylina, M.; Žukovič, M. Stability of skyrmion crystal phase in antiferromagnetic triangular lattice with DMI and single-ion anisotropy. *J. Magn. Magn. Mater.* **2022**, *546*, 168840. [[CrossRef](#)]
43. Berg, B.; Lüscher, M. Definition and statistical distributions of a topological number in the lattice O(3) σ -model. *Nucl. Phys. B* **1981**, *190*, 412–424. [[CrossRef](#)]
44. Zhang, X.; Zhou, Y.; Song, K.M.; Park, T.E.; Xia, J.; Ezawa, M.; Liu, X.; Zhao, W.; Zhao, G.; Woo, S. Skyrmion-electronics: Writing, deleting, reading and processing magnetic skyrmions toward spintronic applications. *J. Phys. Condens. Matter* **2020**, *32*, 143001. [[CrossRef](#)]
45. Creutz, M. Overrelaxation and monte carlo simulation. *Phys. Rev. D* **1987**, *36*, 515. [[CrossRef](#)]
46. Swendsen, R.H.; Wang, J.S. Nonuniversal critical dynamics in Monte Carlo simulations. *Phys. Rev. Lett.* **1987**, *58*, 86. [[CrossRef](#)]
47. Mohylina, M.; Žukovič, M. Effect of impurities on stability of the skyrmion phase in a frustrated heisenberg antiferromagnet. In Proceedings of the 36th International ECMS International Conference on Modelling and Simulation, ECMS, Alesund, Norway, 30 May–3 June 2022.

48. Subbaraman, K.; Zaspel, C.; Drumheller, J.E. Impurity-pinned solitons in the two-dimensional antiferromagnet detected by electron paramagnetic resonance. *Phys. Rev. Lett.* **1998**, *80*, 2201. [[CrossRef](#)]
49. Pereira, A.; Pires, A. Solitons in the presence of a static spin vacancy on a 2D Heisenberg antiferromagnet. *J. Magn. Magn. Mater.* **2003**, *257*, 290–295. [[CrossRef](#)]

Disclaimer/Publisher’s Note: The statements, opinions and data contained in all publications are solely those of the individual author(s) and contributor(s) and not of MDPI and/or the editor(s). MDPI and/or the editor(s) disclaim responsibility for any injury to people or property resulting from any ideas, methods, instructions or products referred to in the content.